ACS Photonics

pubs.acs.org/journal/apchd5

Article

Transfer Matrix Method-Compatible Model for Metamaterial Stacks

Jung-Hwan Song,* Philippe Lalanne, Min-Kyo Seo, and Mark L. Brongersma*

Cite This: https://doi.org/10.1021/acsphotonics.3c00693

Read Online

ACCESS | Metrics & More | Article Recommendations | Supporting Information

ABSTRACT: Mean-field theory-based effective refractive index models are widely used to design optical metamaterials and interpret their optical properties. However, emerging applications where metamaterials are embedded into layered device architectures require a detailed consideration of the metamaterial's dispersive properties and interfacial boundary conditions, which are beyond the scope of the mean-field theory for homogeneous bulk media. Here, we describe an approach to calculate the optical transfer function for one-dimensional optical metamaterials that includes the dispersive properties of the effective index as well as the effective interfacial impedance. We address the boundary conditions at a metamaterial interface by a complex-valued effective interfacial impedance. Combined with the effective refractive index, the effective interfacial impedance enables a description of the optical transfer for 1D optical metamaterials with the transfer matrix method. This opens up scalable design of one-dimensional multilayered structures that include metamaterial layers. We illustrate the approach with the design of a metamaterial-based antireflection coating for a thin-film photodetector.

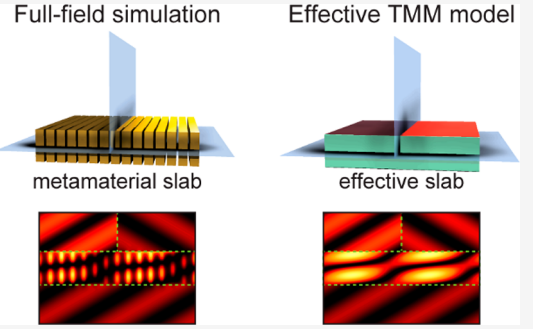

KEYWORDS: *metamaterial, metasurface, nanophotonics, optics, geometrical optics, optical systems, effective medium theory*

INTRODUCTION

Artificially engineered optical metamaterials composed of dense arrays of subwavelength nanostructures have demonstrated properties that go beyond those found in nature. Over the past decades, these materials have been intensively investigated to realize a variety of novel optical functionalities and devices, including negative refraction,[1,2] fluorescence enhancement,[3] spatial wavefront control,[4−8] and flat optical elements.[9−12] The application of such metasurfaces in commercial systems, where conventional optical elements (lenses, prisms, etc.) are combined with conventional materials and metamaterials, requires simulation tools capable of handling multiple very disparate length scales and distinct types of optical physics. At large length scales, the use of ray-tracing software can be very fruitful, while full-field simulations are needed to accurately model the flow of light through the nanostructured metamaterials. Currently, there are no commercial packages that efficiently handle these problems. If this can be achieved, it will allow for a more convenient, intuitive, and computationally less expensive design. It will also facilitate the use of emerging optical simulation techniques based on inverse and topological optimization to realize high-performance metamaterial-based systems. Here, we show an approach that will open the possibility to combine ray-tracing and full-field simulations via rigorous coupled wave analysis (RCWA) in a convenient transfer-matrix method (TMM). The RCWA simulations are used to calculate effective indices and interfacial impedances of the metamaterial layers and interfaces. In doing so, this technique allows for a more simplified analysis by hiding the complex optical properties of the artificial media in a small set of effective parameters. A central goal in the research on optical metamaterials and metasurfaces has been to replace conventional bulky optical elements and layers in optoelectronic devices.[13−15] To this end, it is critical to understand and capture how their optical behavior depends on the incident angle, polarization, and wavelength of the incoming light. Based on this observation, it is convenient to employ Fourier engineering in the design of these elements.[9,11] The importance of the incident angle of light (i.e., encoded in the k-vector) is particularly relevant for metamaterials with spatially nonlocal optical resonances, which operate directly in the momentum domain.[16−18] Utilization of such nonlocal metamaterials and metasurfaces is now giving birth to a new generation of flat, Fourier optical devices such as optical analog computers[19,20] and image processors.[21−23] Understanding the effective optical response and creating new functionalities in the Fourier domain, however, require more than what a mean-field theory can deliver. The mean-field model ensures the valid results only for a limited set of conditions in terms of the incident angle, polarization, and wavelength.[24] Moreover, the macroscopic boundary conditions

Received: May 23, 2023

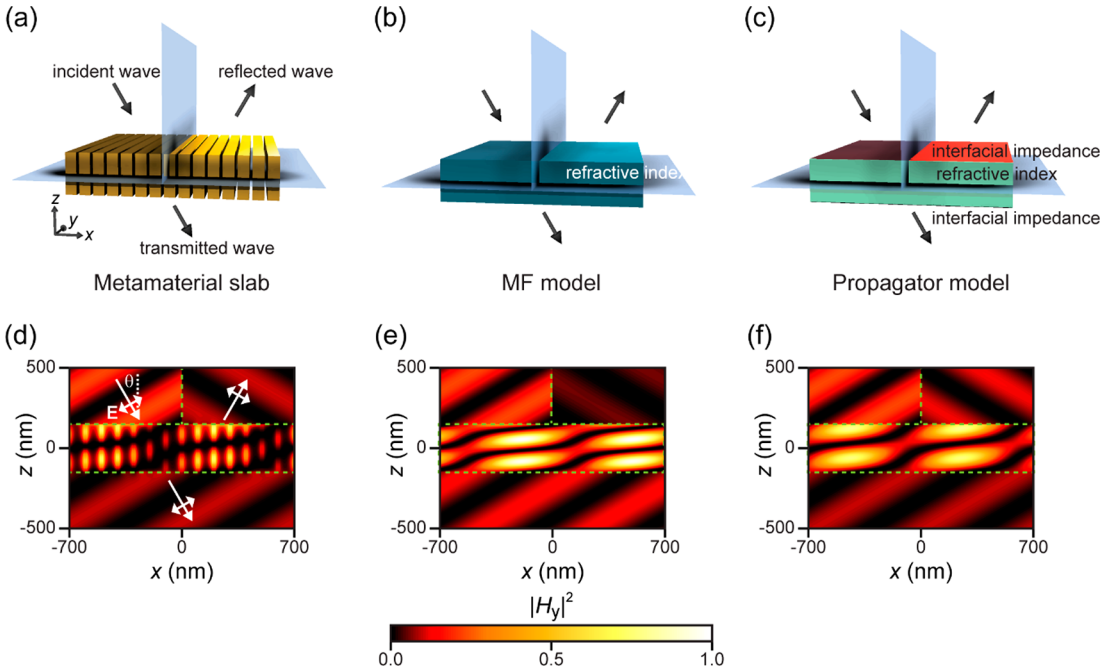

Figure 1. Accurate, scalable effective refractive index and interfacial impedance model that can be used in conjunction with the transfer matrix method (TMM). (a–c) Schematics of an exemplar optical metamaterial (a) and corresponding effective media derived from a mean-field (MF) model (b) and a propagator model (c). The propagator model includes not only the effective refractive index of the layers, but also the relevant effective interfacial impedances. (d–f) The magnetic field intensity profiles obtained from a rigorous coupled wave analysis (RCWA) of the actual metamaterial (d), TMM calculation employing the effective refractive index from the MF model (e), and TMM calculation employing the effective refractive index and interfacial impedance of our propagator model (f). θ is the incident angle (=30°) of the planewave with TM polarization (x and z electric field components). The wave inside the metamaterial slab as well as the incident, reflected, and transmitted waves are displayed. For the subpanels showing the reflected waves (top right), we extract the reflected fields by subtracting the incident fields from the total fields. The period of the metamaterial is 100 nm, and the thickness of the slab is arbitrarily chosen to be 300 nm. The width of the Au ridge is 80 nm.

based only on the effective refractive index fail to accurately predict the amplitude and phase of the transmitted and reflected fields at metamaterial interfaces.[25]

To build a model that includes dispersion, it is worth looking back to the earlier work by Kronig and Penney on the electron band structures in solid-state physics.[26] They obtained the coupled Eigen solutions for the electron states in a crystal medium by imposing periodic boundary conditions. Recently, the Kronig–Penney (KP) model was applied to an investigation of the dispersive properties and Purcell effect in periodic metal and dielectric metamaterials.[27−29] The propagation constant of weakly coupled surface plasmon polariton solutions can capture the light-propagation behavior in the metamaterials in a rigorous, exact manner. In order to also take the unpredictable optical amplitude and phase at the interface of optical metamaterials into account, we develop the concept of effective interfacial impedance as a function of the angle of incidence, wavelength, and polarization. We provide a versatile, scalable propagator model (P. M.) by incorporating the KP effective refractive index and our proposed effective interfacial impedance into the conventional TMM formalism. As a proof-of-concept, a tutorial optimization process for an antireflective, conductive coating on a heterostructure with intrinsic thin layer (HIT) photodetector is demonstrated. We expect that, due to the TMM-compatibility and scalability, our propagator model will be a promising tool for the design and analysis of functional metamaterial systems involving multiple layers.

RESULTS AND DISCUSSION

To explore the validity of our suggested approach, we first describe a stereotypical example in which a metamaterial slab is illuminated with a polarized planewave. Figure 1a illustrates the 300 nm thick slab with a periodic metal (Au)–dielectric (SiO_2) structure. We investigate the reflection and transmission of this slab embedded in a uniform dielectric environment (SiO_2) as a function of the polarization state, angle of incidence, period, and filling fraction of the Au ridge. Figure 1b and c present the effective slab structures by the mean-field model and our propagator model, respectively. To explore the validity of our approach, we first analyze a 300 nm thick metamaterial slab under planewave illumination with transverse magnetic (TM) polarized (i.e., p-polarized) light. Figure 1d–f shows the magnetic field intensity profiles obtained with a rigorous coupled-wave analysis (RCWA) simulator[30−32] and corresponding TMM calculations employing the mean-field model and our propagator model. Here, the wavelength of light and incident angle are 1 μm and 30°, respectively. We set the dielectric constants of Au[33] and SiO_2 to be $-42.63 + 3.32i$ and 2.10.

The example system exposes several limitations of the conventional mean-field model. It clearly lacks accuracy in calculating the amplitude and phase of the reflected and transmitted waves. The local field intensity profile inside the metamaterial slab by this model (Figure 1e) also shows significant deviations in the propagation angle and number of nodal planes inside the slab from those obtained by the RCWA simulations (Figure 1d). Even if the effective refractive index were calculated correctly, one cannot ignore the interfacial

https://doi.org/10.1021/acsphotonics.3c00693
ACS Photonics XXXX, XXX, XXX−XXX

impedance in matching the boundary conditions at the interface between the structured metamaterial and the surrounding homogeneous medium. Knowledge of the interfacial impedance is needed to accurately calculate the transmitted and reflected fields. In this study, we employ the KP effective refractive index and effective interfacial impedance and plug them into the TMM formalism. As shown in Figure 1f, our propagator model-based TMM calculation accurately predicts not only the amplitude and phase of the reflected and transmitted waves but also the locations and the intervals of the nodal planes inside the metamaterial. The same results hold for the TE polarization (*s*-polarization) as well (not shown).

We first calculated the effective refractive index defined by the ratio of the *z*-component of the wave vector inside the metamaterial (β_z) to that in the air (k_0): $n_{eff} + ik_{eff} = \beta_z/k_0$.[24] The effective refraction angle in the effective medium, θ_p is given by $\tan^{-1}(\beta_x/\mathrm{Re}[\beta_z])$ (Figure 2a). The period of the 1D metamaterial, the width of the Au ridge, and the width of the SiO_2 ridge are denoted as *p*, *w*, and *a*, respectively. By employing Bloch's theorem, the effective refractive index for TM polarization is obtained by calculating the roots of the following equation[34]

$$\left\{\left(\frac{\kappa_1}{\varepsilon_1}\right)^2 + \left(\frac{\kappa_2}{\varepsilon_2}\right)^2\right\}\{\cosh(\kappa_1 a + \kappa_2 w) - \cosh(\kappa_2 a - \kappa_2 w)\} + \frac{2\kappa_1\kappa_2}{\varepsilon_1\varepsilon_2}\{\cosh(\kappa_1 a + \kappa_2 w) + \cosh(\kappa_2 a - \kappa_2 w) - 2\cos(\beta_x p)\} = 0 \quad (1)$$

where κ_j is $(\beta_z^2 - \omega^2/c^2\varepsilon_j)^{1/2}$ and the Bloch phase factor is $\exp(i\beta_x x)$. Meanwhile, the equation for the TE polarization is as follows:

$$\{\kappa_1^2 + \kappa_1^2\}\{\cosh(\kappa_1 a + \kappa_2 w) - \cosh(\kappa_2 a - \kappa_2 w)\} + 2\kappa_1\kappa_2\{\cosh(\kappa_1 a + \kappa_2 w) + \cosh(\kappa_2 a - \kappa_2 w) - 2\cos(\beta_x p)\} = 0 \quad (2)$$

We note that advanced numerical methods such as RCWA[30] can be used to obtain the effective refractive index in more general, multidimensional periodic structures.[12,35] The zeroth-order of the effective refractive index obtained by the mean-field model is the arithmetic or harmonic mean of the dielectric constants[24] of Au and SiO_2 weighted by the filling fraction of the Au ridge.

Figure 2b shows the effective refractive index for the TM polarization as a function of the width of the Au ridge and the wave vector along the *x*-axis. The dominance of the real part of the effective refractive index reflects that the metamaterial supports propagating modes for TM polarization. As observed in Figure 1d, the light in the metamaterial propagates along the *z*-direction through an array of SiO_2 ridges. The evanescent field decays along the *x*-direction in the Au ridge featuring a coupled metal−dielectric−metal (MIM) waveguide mode. The monotonic increase of the effective refractive index as a function of the width of the Au ridge is consistent with the basic trend of the modal index of a MIM waveguide as decreasing the width of dielectric core (SiO_2 ridge). The angle dependence of the effective refractive index manifests hyperbolic dispersion characteristics.[36] While the KP model provides results consistent with the RCWA calculations, the mean-field model loses its validity as the width of the Au ridge gets larger or the propagation angle increases. In these cases, the evanescent field from a SiO_2 ridge rapidly decays across the

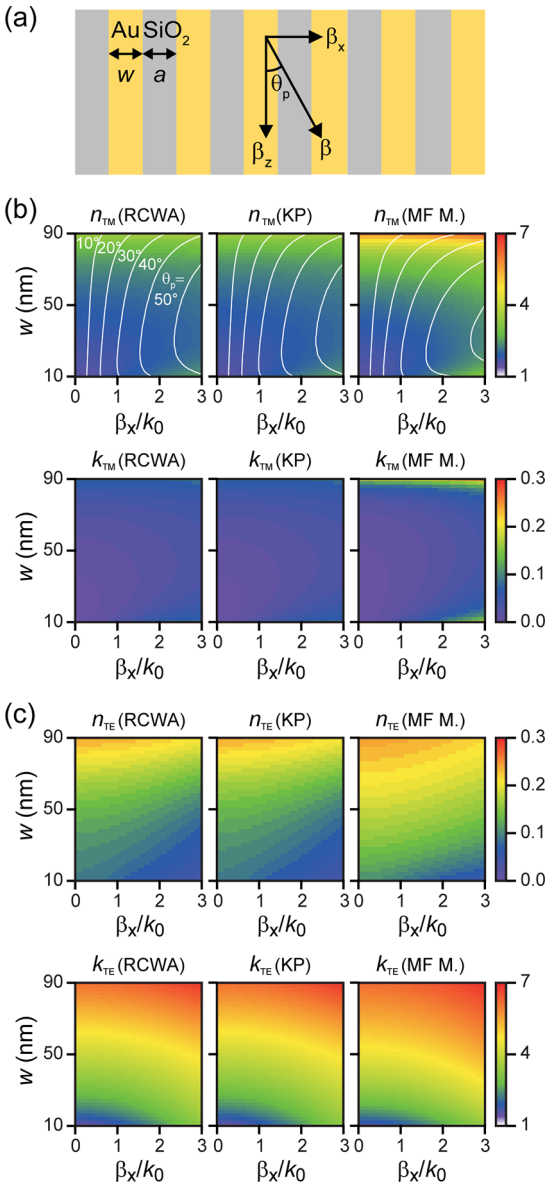

Figure 2. Effective refractive index. (a) Schematic of the wave propagation of a one-dimensional metal−dielectric metamaterial. The period of the metamaterial and the wavelength of light are 100 nm and 1 μm, respectively. (b) The complex effective refractive index for the transverse magnetic (TM) polarization (*p*-polarization), as calculated by the RCWA method, the Kronig−Penny model (KP), and the mean-field model (MF M.), respectively. The effective refractive index is plotted as a function of the width of Au ridge (w) and the x component of the wave vector (β_x) The solid white lines indicate the equi-propagation angle inside the metamaterial medium from 10° to 50°. (c) The complex-valued effective refractive index for the transverse-electric (TE) polarization (*s*-polarization).

Au ridge before it reaches the neighboring SiO_2 ridges. As a result, each SiO_2 ridge behaves as an almost isolated MIM waveguide. This significantly reduces the field homogeneity that is assumed in the mean-field theory.[24] For the TE polarization (Figure 2c), the metamaterial behaves as a metallic medium, of which the complex permittivity has a negative real number (i.e., imaginary part-dominant effective refractive index). This behavior is closely related to the cutoff of a planar mirror waveguide with a subwavelength-wide dielectric core. The narrower the width of the SiO_2 ridge, the more rapid

https://doi.org/10.1021/acsphotonics.3c00693
ACS Photonics XXXX, XXX, XXX−XXX

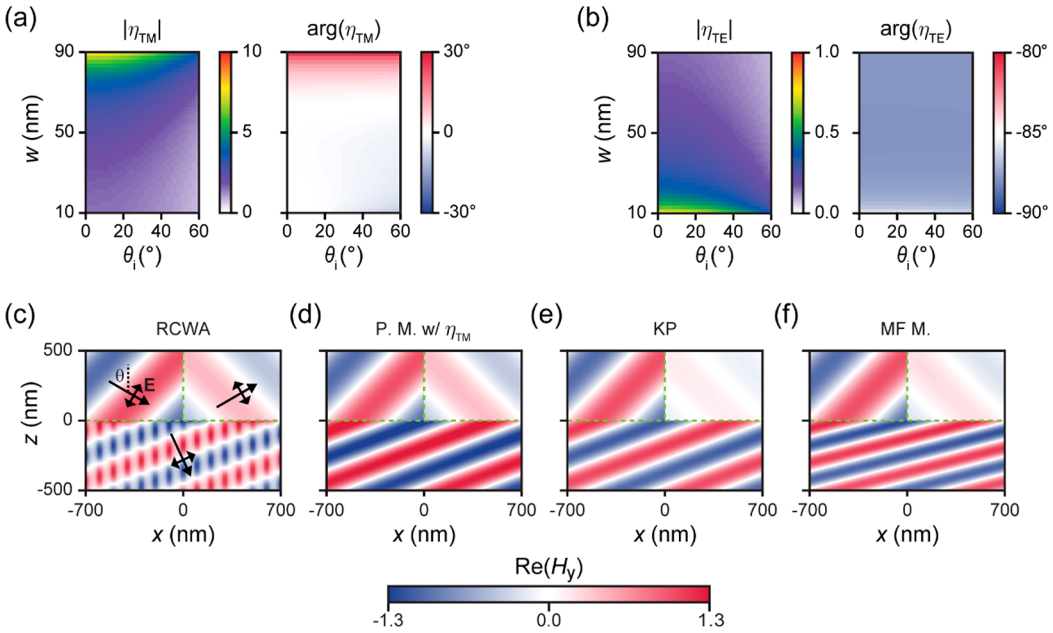

Figure 3. Effective interfacial impedance. (a, b) Calculated absolute values of effective interfacial impedance ratio at the interface from the air to the metal-dielectric metamaterial depending on the width of Au ridge (w) and incident angle (θ) for the (a) TM and (b) TE polarization states. The period of the metamaterial is fixed to 100 nm. (c–f) Field profiles of the incident, reflected, and refracted fields for the TM polarization obtained by RCWA simulations (c). TMM calculations employing both the effective interfacial impedance and the effective refractive index of our propagator model (d), only the effective refractive index from the KP model (e), and the effective refractive index from the MF model (f), respectively. Here, the incident angle is set to 45° and the y-component of the magnetic field is plotted.

the evanescent propagation along the z-direction, which can explain the increasing trend of the imaginary part of the effective refractive index as a function of the width of the Au ridge. As is the case for the TM polarization, the mean-field model for the TE polarization is valid when the Au ridge is sufficiently thin. However, the KP model intrinsically addresses the inhomogeneity of the fields and thus provides the exact effective refractive index of the metamaterial within the valid region of single-mode propagation (see Supporting Information, Figure S1).

Different from homogeneous media, it is not trivial to apply the effective refractive index of a metamaterial to macroscopic boundary conditions at its interface with another medium.[25,37,38] The effective refractive index alone determines the refraction angle and phase velocity, but fails to calculate the phase shift and amplitude of the reflected and transmitted waves. Here, we show that the boundary conditions at the interface between a metal–dielectric metamaterial and a homogeneous medium can be precisely interpreted by introducing the concept of effective interfacial impedance. Further, it is compatible with TMM calculations in the form of an interface matrix.

The latter can be computed with advanced numerical tools by expanding the fields of both media in their respective modal bases (plane waves for the homogeneous medium and Bloch modes for the metamaterial) and by further matching the tangential electromagnetic field components at the interface.[39] By solving the boundary conditions, the scattering interfacial matrix that links the outgoing mode amplitudes to the ingoing ones is computed. The electromagnetic response of single interfaces can thus be rigorously modeled by considering all evanescent modes in both media. The approach has been successfully implemented to study the property of high-index lamellar gratings[29] or, more closely related to the present example, interfaces between homogeneous media and metallic hole arrays.[39] It provides a deep insight into the homogenization process, does not introduce any approximation, but requires advanced numerical tools that are comparatively as complicated as the RCWA.

Hereafter, we introduce a simplified formalism which relies on the sole knowledge of a complex-valued reflection coefficient r from which we infer all of the properties of the interface. Indeed, the approach contains an approximate treatment of the transmission coefficient between the modes of the interfacial materials. The coefficient is inferred from the reflection coefficient by assuming that the interfacial impedance is that between two uniform media. This approach, admittedly approximate, has the advantage of being directly implementable without any modification of a grating code, such as the RCWA. We will see that it can be very precise.

With our approximation and for the TM-polarized incidence, we define a modified interface matrix for the magnetic field (H_y field) from a medium i to t given as follows:

$$D_{i\to t} = \frac{1}{2}\begin{bmatrix} 1+\eta_{i\to t}(\theta_i) & 1-\eta_{i\to t}(\theta_i) \\ 1-\eta_{i\to t}(\theta_i) & 1+\eta_{i\to t}(\theta_i) \end{bmatrix} \quad (3)$$

Here, we define $\eta_{i\to t}$ as the interfacial impedance ratio from an incident medium i to a transmitting medium t as a function of the incident angle. In this study, we retrieve the modified interface matrix between a metamaterial medium and a homogeneous medium through full-field simulations (RCWA). We first calculate a reflection coefficient (r) by simulating a planewave incidence from the semi-infinite homogeneous dielectric medium to the semi-infinite metamaterial medium. Applying eq 3 for such a single interface, we obtain the interfacial impedance ratio ($\eta_{i\to t}$) as a rational polynomial function of r at each incident angle (θ_i):

https://doi.org/10.1021/acsphotonics.3c00693
ACS Photonics XXXX, XXX, XXX–XXX

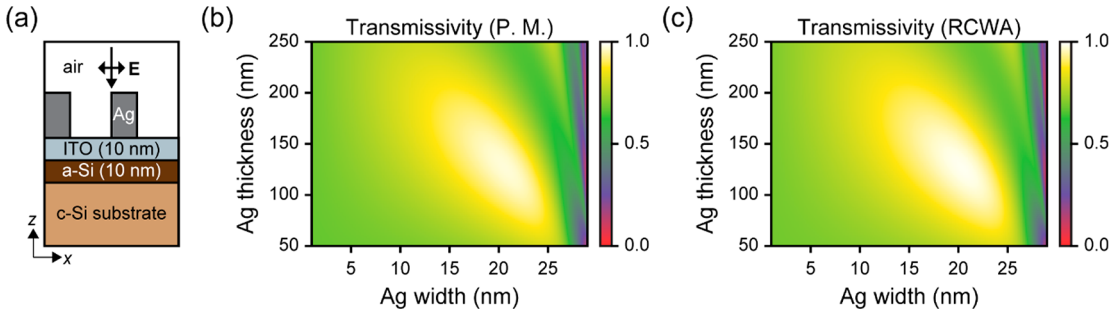

Figure 4. Optimization of an antireflecting plasmonic metasurface for a heterojunction with intrinsic thin layer (HIT) photodetector. (a) Cross section of two photonic unit cells of the proposed plasmonic metasurface structure that serves as an antireflection coating. (b) Two-dimensional map of the transmissivity into the c-Si substrate as a function of the Ag width and Ag thickness, as obtained by our propagator model. The wavelength is set to 1 μm, and the polarization is along the x direction (TM polarization). The period of the plasmonic metasurface is fixed to 30 nm. (c) 2D map of the transmissivity calculated by RCWA simulations.

$$\eta_{i\to t}(\theta_i) = \frac{1 + r(\theta_i)}{1 - r(\theta_i)} \tag{4}$$

The use of r from the full-field simulations allows the resultant modified interface matrix to derive the valid optical transfer functions at the interfaces as accurately as those from the full-field simulations. Once determined, the effective interfacial impedance ratio of a certain interface can be plugged into the TMM calculation for any stratified structures including the identical interface without additional numerical simulations, which demonstrates the scalability of our model. We note that there are also semianalytical studies on such interfacial impedance[37,40−42] based on eigenmode decomposition methods. Both our numerical and the semianalytical methods would give equivalent results when the eigenmodes at the interface resemble a planewave.[37]

Figure 3a and b show the extracted interfacial impedance ratio at the interface between the homogeneous incident medium (air) and the metamaterial transmitting medium for the TM and TE polarization states, respectively. For TM polarization, the interfacial impedance ratio (η_{TM}) represents the refractive index of the metamaterial. The monotonic trend of the amplitude and phase of η_{TM} (Figure 3a) as a function of the angle of incidence and the width of the Au ridge is consistent with that of its effective refractive index in Figure 2b. For the TE polarization, η_{TE} represents the inverse of the refractive index. η_{TE} shows even better quantitative agreement with the inverse of the effective refractive index (Figure 2c). This is because the electric field is tangential for this polarization, which guarantees the continuity across the boundary between the Au and SiO_2 ridges in the metamaterial. For this reason, even the mean-field theory-based effective refractive index is quite good at predicting the optical transfer properties.

The comparison of the RCWA simulations and TMM calculations clarifies the effectiveness and validity of the effective interfacial impedance (Figure 3c−f). The TMM calculation employing both the effective interfacial impedance and the KP effective refractive index accurately reproduces the propagation angle, the amplitude, and the phase of the reflected and refracted waves by the RCWA simulations (compare Figure 3c,d). On the other hand, the TMM calculation employing only the KP effective refractive index of the propagator model yields inaccurate amplitudes of the reflected and refracted waves (Figure 3e). Besides, the TMM calculation employing the mean-field model does not predict either the amplitudes of the waves or the propagation angle inside the metamaterial, as depicted in Figure 3f (see also Supporting Information, Figure S2).

To demonstrate the advantage and reliability of our TMM-compatible model in multilayered system designs, we investigate a plasmonic metasurface on a HIT photodetector as a tutorial example (Figure 4a). Here, the metasurface, a thin slab of the metal (Ag)−dielectric (air) periodic metamaterial, not only acts as a top electrode, but also enhances the transmission of incident light into the crystalline silicon (c-Si) layer, which would improve the generation and harvesting of the photocarriers. Typical HIT solar cells[43] have employed an indium tin oxide (ITO) layer with a thickness of ∼100 nm as a transparent conductive layer. However, such a thick ITO layer still has a relatively poor sheet resistance[44] as well as nonnegligible intrinsic light absorption.[45,46] Inspired by the applications of agglomerated metallic nanostructures to improve the sheet resistance and heat durability of transparent conductive layer,[47−49] we suggest a plasmonic metasurface which can enhance the electrical/heat conduction and boost the light transmission into the c-Si substrate at the same time.

The HIT photodetector examined in this study consists of a plasmonic Ag metasurface, thin ITO, amorphous silicon (a-Si), and c-Si layers. We calculate the transmissivity into the c-Si substrate as a function of the width and thickness of the Ag elements of the metasurface for a TM-polarized normal incidence. The two-dimensional transmissivity map in Figure 4b is obtained by the TMM calculations employing the effective refractive index and interfacial impedance of the metasurface, of which the transfer matrix is given by

$$\mathbf{M} = \mathbf{D}_{\text{a-Si}\to\text{c-Si}}\cdot\mathbf{P}_{\text{a-Si}}\cdot\mathbf{D}_{\text{ITO}\to\text{a-Si}}\cdot\mathbf{P}_{\text{ITO}}\cdot\mathbf{D}_{\text{MM}\to\text{ITO}}\cdot\mathbf{P}_{\text{MM}}\cdot\mathbf{D}_{\text{air}\to\text{MM}} \tag{5}$$

$\mathbf{P}_j$ is the propagator matrix for a layer j:

$$\mathbf{P}_j = \begin{bmatrix} e^{i\beta_j d_j} & 0 \\ 0 & e^{-i\beta_j d_j} \end{bmatrix} \tag{6}$$

where β_j and d_j are the propagation constant and thickness of the layer j, respectively. As a comparison, we also plot the 2D transmissivity map obtained by the full-field RCWA simulation in Figure 4c. Notably, the TMM calculations employing the effective refractive index and interfacial impedance precisely reproduce the results of the RCWA simulation regardless of the geometry of the Ag−air metasurface and enable us to

https://doi.org/10.1021/acsphotonics.3c00693
ACS Photonics XXXX, XXX, XXX−XXX

readily get the optimized structure for the given illumination wavelength (λ = 1 μm). We observe the optimized transmission in the proximity of a 20 nm wide, 120 nm thick Ag element, which corresponds to the Fabry−Pérot resonance of the plasmonic metamaterial slab.

An evaluation of the effective refractive index and interfacial impedance not only opens a pathway toward efficient optimization but also generates new, fundamental insights into the operation of a metamaterial medium. The effective refractive index of the Ag metasurface near the maximum transmission condition is 1.8 + 0.005*i*. Nearly positive, real effective refractive index highlights its function as a low-loss dielectric.[50,51] The complex-valued effective interfacial impedances at both the top and bottom of the Ag metasurface indicate that additional phase pickups upon internal light reflection are imprinted. This explains how Fabry−Pérot resonances can emerge even for a sub-$\lambda/2n$ film thickness (120 nm), which, in turn, enables large light transmission (98.8%) into the c-Si substrate with a reduced amount of light absorption and material cost.

CONCLUSIONS

In summary, we investigated the effective refractive index and interfacial impedance of metal−dielectric optical metamaterials and showed that our TMM-compatible propagator model captures all of the features of light propagation, reflection, and refraction through the interfaces between the metamaterials and homogeneous media. The KP model yields the effective refractive index as accurately as the RCWA calculation, regardless of the propagation direction, the polarization state of the wave, and the geometry of metamaterials. Our proposed effective interfacial impedance makes it possible to include the exact boundary conditions between metamaterial and any homogeneous media as an interface matrix in TMM calculations. We were thus able to precisely calculate the optical transfer functions of multilayered structures, including a metamaterial layer of an arbitrary thickness and a tutorial HIT photodetector. The concept of the TMM-compatible, scalable effective refractive index and interfacial impedance will facilitate further understanding of the role of the metamaterial layers in multilayer stacks and provide guidelines for the design of practical flat optical systems.

ASSOCIATED CONTENT

Supporting Information

The Supporting Information is available free of charge at https://pubs.acs.org/doi/10.1021/acsphotonics.3c00693.

Additional figures for explaining the validity of TMM-compatible effective propagator model (Figure S1); Fresnel coefficients of an example metamaterial slab structure obtained by the TMM-compatible approach (Figure S2) (PDF)

AUTHOR INFORMATION

Corresponding Authors

Jung-Hwan Song − *Geballe Laboratory for Advanced Materials, Stanford University, Stanford, California 94305, United States;* orcid.org/0000-0001-9502-5718; Email: vsong21@stanford.edu

Mark L. Brongersma − *Geballe Laboratory for Advanced Materials, Stanford University, Stanford, California 94305, United States;* orcid.org/0000-0003-1777-8970; Email: brongersma@stanford.edu

Authors

Philippe Lalanne − *LP2N, Institut d'Optique Graduate School, CNRS, Université de Bordeaux, Talence 33400, France;* orcid.org/0000-0003-1979-2290

Min-Kyo Seo − *Department of Physics, Korea Advanced Institute of Science and Technology, Daejeon 34141, Republic of Korea;* orcid.org/0000-0003-0618-3955

Complete contact information is available at: https://pubs.acs.org/10.1021/acsphotonics.3c00693

Funding

NRF-2016R1A6A3A03012480; NRF-2020R1A2C2014685; FA9550-21-1-0312; DE-FG07-ER46426.

Notes

The authors declare no competing financial interest.

ACKNOWLEDGMENTS

J.-H.S. is supported by Basic Science Research Program through the National Research Foundation of Korea (NRF-2016R1A6A3A03012480). M.-K.S. acknowledges support by the National Research Foundation of Korea (NRF-2020R1A2C2014685). M.L.B. was supported by a MURI program of the United States Air Force Office of Scientific Research (Grant No. FA9550-21-1-0312) and a grant from the Department of Energy (Grant No. DE-FG07-ER46426).

REFERENCES

(1) Pendry, J. B. Negative Refraction Makes a Perfect Lens. *Phys. Rev. Lett.* **2000**, *85* (18), 3966−3969.

(2) Smith, D. R.; Pendry, J. B.; Wiltshire, M. C. K. Metamaterials and Negative Refractive Index. *Science* **2004**, *305*, 788−792.

(3) Lu, D.; Kan, J. J.; Fullerton, E. E.; Liu, Z. Enhancing Spontaneous Emission Rates of Molecules Using Nanopatterned Multilayer Hyperbolic Metamaterials. *Nat. Nanotechnol.* **2014**, *9* (1), 48−53.

(4) Huang, Y. W.; Lee, H. W. H.; Sokhoyan, R.; Pala, R. A.; Thyagarajan, K.; Han, S.; Tsai, D. P.; Atwater, H. A. Gate-Tunable Conducting Oxide Metasurfaces. *Nano Lett.* **2016**, *16* (9), 5319−5325.

(5) Park, J.; Kang, J. H.; Kim, S. J.; Liu, X.; Brongersma, M. L. Dynamic Reflection Phase and Polarization Control in Metasurfaces. *Nano Lett.* **2017**, *17* (1), 407−413.

(6) Sun, J.; Timurdogan, E.; Yaacobi, A.; Hosseini, E. S.; Watts, M. R. Large-Scale Nanophotonic Phased Array. *Nature* **2013**, *493* (7431), 195−199.

(7) Shaltout, A. M.; Lagoudakis, K. G.; van de Groep, J.; Kim, S. J.; Vučković, J.; Shalaev, V. M.; Brongersma, M. L. Spatiotemporal Light Control with Frequency-Gradient Metasurfaces. *Science* **2019**, *365* (6451), 374−377.

(8) Park, J.; Jeong, B. G.; Kim, S. I.; Lee, D.; Kim, J.; Shin, C.; Lee, C. B.; Otsuka, T.; Kyoung, J.; Kim, S.; Yang, K.-Y.; Park, Y.-Y.; Lee, J.; Hwang, I.; Jang, J.; Song, S. H.; Brongersma, M. L.; Ha, K.; Hwang, S.-W.; Choo, H.; Choi, B. L. All-Solid-State Spatial Light Modulator with Independent Phase and Amplitude Control for Three-Dimensional LiDAR Applications. *Nat. Nanotechnol.* **2021**, *16* (1), 69−76.

(9) Brongersma, M. L. The Road to Atomically Thin Metasurface Optics. *Nanophotonics* **2020**, *10* (1), 643−654.

(10) Lin, D.; Fan, P.; Hasman, E.; Brongersma, M. L. Dielectric Gradient Metasurface Optical Elements. *Science* **2014**, *345* (6194), 298−302.

(11) Chen, W. T.; Zhu, A. Y.; Capasso, F. Flat Optics with Dispersion-Engineered Metasurfaces. *Nature Reviews Materials* **2020**, *5*, 604−620.

(12) Lalanne, P.; Astilean, S.; Chavel, P.; Cambril, E.; Launois, H. Blazed Binary Subwavelength Gratings with Efficiencies Larger than Those of Conventional Échelette Gratings. *Opt. Lett.* **1998**, *23* (14), 1081.
(13) Atwater, H. A.; Polman, A. Plasmonics for Improved Photovoltaic Devices. *Nat. Mater.* **2010**, *9*, 205.
(14) Joo, W. J.; Kyoung, J.; Esfandyarpour, M.; Lee, S. H.; Koo, H.; Song, S.; Kwon, Y. N.; Song, S. H.; Bae, J. C.; Jo, A.; Kwon, M. J.; Han, S. H.; Kim, S. H.; Hwang, S.; Brongersma, M. L. Metasurface-Driven OLED Displays beyond 10,000 Pixels per Inch. *Science* **2020**, *370* (6515), 459−463.
(15) Dorrah, A. H.; Capasso, F. Tunable Structured Light with Flat Optics. *Science* **2022**, *376* (6591). DOI: 10.1126/science.abi6860.
(16) Guo, C.; Wang, H.; Fan, S. Squeeze Free Space with Nonlocal Flat Optics. *Optica.* **2020**, *7*, 1133.
(17) Lawrence, M.; Barton, D. R.; Dixon, J.; Song, J.-H.; van de Groep, J.; Brongersma, M. L.; Dionne, J. A. High Quality Factor Phase Gradient Metasurfaces. *Nat. Nanotechnol.* **2020**, *15* (11), 956−961.
(18) Overvig, A. C.; Malek, S. C.; Yu, N. Multifunctional Nonlocal Metasurfaces. *Phys. Rev. Lett.* **2020**, *125* (1), No. 017402.
(19) Pors, A.; Nielsen, M. G.; Bozhevolnyi, S. I. Analog Computing Using Reflective Plasmonic Metasurfaces. *Nano Lett.* **2015**, *15* (1), 791−797.
(20) Silva, A.; Monticone, F.; Castaldi, G.; Galdi, V.; Alù, A.; Engheta, N. Performing Mathematical Operations with Metamaterials. *Science* **2014**, *343* (6167), 160−163.
(21) Cordaro, A.; Kwon, H.; Sounas, D.; Koenderink, A. F.; Alù, A.; Polman, A. High-Index Dielectric Metasurfaces Performing Mathematical Operations. *Nano Lett.* **2019**, *19* (12), 8418−8423.
(22) Zhu, T.; Zhou, Y.; Lou, Y.; Ye, H.; Qiu, M.; Ruan, Z.; Fan, S. Plasmonic Computing of Spatial Differentiation. *Nat. Commun.* **2017**, *8* (1), 15391.
(23) Zhou, Y.; Zheng, H.; Kravchenko, I. I.; Valentine, J. Flat Optics for Image Differentiation. *Nat. Photonics* **2020**, *14* (5), 316−323.
(24) Benisty, H.; Greffet, J.-J.; Lalanne, P. *Introduction to Nanophotonics*; Oxford University Press, 2022, chap. 15.
(25) Smith, D. R.; Schultz, S.; Markoš, P.; Soukoulis, C. M. Determination of Effective Permittivity and Permeability of Metamaterials from Reflection and Transmission Coefficients. *Phys. Rev. B* **2002**, *65* (19), No. 195104.
(26) de L. Kronig, R.; Penney, W. G. Quantum Mechanics of Electrons in Crystal Lattices. *Proc. R. Soc. A Math. Phys. Eng. Sci.* **1931**, *130* (814), 499−513.
(27) Chebykin, A. V.; Orlov, A. A.; Vozianova, A. V.; Maslovski, S. I.; Kivshar, Y. S.; Belov, P. A. Nonlocal Effective Medium Model for Multilayered Metal-Dielectric Metamaterials. *Phys. Rev. B* **2011**, *84* (11), No. 115438.
(28) Li, T.; Khurgin, J. B. Hyperbolic Metamaterials : Beyond the Effective Medium Theory. *Optica* **2016**, *3* (12), 1388−1396.
(29) Lalanne, P.; Hugonin, J. P.; Chavel, P. Optical Properties of Deep Lamellar Gratings: A Coupled Bloch-Mode Insight. *J. Light. Technol.* **2006**, *24* (6), 2442−2449.
(30) Moharam, M. G.; Gaylord, T. K.; Grann, E. B.; Pommet, D. A. Formulation for Stable and Efficient Implementation of the Rigorous Coupled-Wave Analysis of Binary Gratings. *J. Opt. Soc. Am. A* **1995**, *12* (5), 1068−1076.
(31) Zhao, B.; Zhang, Z. M. Study of Magnetic Polaritons in Deep Gratings for Thermal Emission Control. *J. Quant. Spectrosc. Radiat. Transfer* **2014**, *135*, 81−89.
(32) Lalanne, P.; Morris, G. M. Highly Improved Convergence of the Coupled-Wave Method for TM Polarization. *J. Opt. Soc. Am. A* **1996**, *13* (4), 779−784.
(33) Johnson, P. R.; Christy, R. W. Optical Constants of the Noble Metals. *Phys. Rev. B. Solid State* **1972**, *6* (12), 4370.
(34) Rytov, S. Electromagnetic Properties of a Finely Stratified Medium. *Sov. Phys. JEPT* **1956**, *2*, 466−475.
(35) Hugonin, J.-P.; Lalanne, P. RETICOLO Software for Grating Analysis. *arXiv.2101.00901* **2021**, na.
(36) Yang, X.; Yao, J.; Rho, J.; Yin, X.; Zhang, X. Experimental Realization of Three-Dimensional Indefinite Cavities at the Nanoscale with Anomalous Scaling Laws. *Nat. Photonics* **2012**, *6* (7), 450−454.
(37) Paul, T.; Menzel, C.; Smigaj, W.; Rockstuhl, C.; Lalanne, P.; Lederer, F. Reflection and Transmission of Light at Periodic Layered Metamaterial Films. *Phys. Rev. B: Condens. Matter Mater. Phys.* **2011**, *84* (11), No. 115142.
(38) Yang, J.; Sell, D.; Fan, J. A. Freeform Metagratings Based on Complex Light Scattering Dynamics for Extreme, High Efficiency Beam Steering. *Ann. Phys.* **2018**, *530* (1), No. 1700302.
(39) Lalanne, P.; Rodier, J. C.; Hugonin, J. P. Surface Plasmons of Metallic Surfaces Perforated by Nanohole Arrays. *J. Opt. A Pure Appl. Opt.* **2005**, *7* (8), 422−426.
(40) Lalanne, P.; Hugonin, J. P.; Astilean, S.; Palamaru, M.; Möller, K. D. One-Mode Model and Airy-like Formulae for One-Dimensional Metallic Gratings. *J. Opt. A Pure Appl. Opt.* **2000**, *2* (1), 48−51.
(41) Yang, J.; Sauvan, C.; Paul, T.; Rockstuhl, C.; Lederer, F.; Lalanne, P. Retrieving the Effective Parameters of Metamaterials from the Single Interface Scattering Problem. *Appl. Phys. Lett.* **2010**, *97* (6), No. 061102.
(42) McPhedran, R. C.; Maystre, D. On the Theory and Solar Application of Inductive Grids. *Appl. Phys.* **1977**, *14*, 1−20.
(43) Taguchi, M.; Terakawa, A.; Maruyama, E.; Tanaka, M. Obtaining a Higher Voc in HIT Cells. *Prog. Photovoltaics Res. Appl.* **2005**, *13* (6), 481−488.
(44) Jin, H.; Tao, C.; Velusamy, M.; Aljada, M.; Zhang, Y.; Hambsch, M.; Burn, P. L.; Meredith, P. Efficient, Large Area ITO-and-PEDOT-Free Organic Solar Cell Sub-Modules. *Adv. Mater.* **2012**, *24* (19), 2572−2577.
(45) Chao, Y.; Tang, W.; Wang, X. Properties of Resistivity, Reflection and Absorption Related to Structure of ITO Films. *J. Mater. Sci. Technol.* **2012**, *28* (4), 325−328.
(46) König, T. A. F.; Ledin, P. A.; Kerszulis, J.; Mahmoud, M. A.; El-Sayed, M. A.; Reynolds, J. R.; Tsukruk, V. V. Electrically Tunable Plasmonic Behavior of Nanocube-Polymer Nanomaterials Induced by a Redox-Active Electrochromic Polymer. *ACS Nano* **2014**, *8* (6), 6182−6192.
(47) Garnett, E. C.; Cai, W.; Cha, J. J.; Mahmood, F.; Connor, S. T.; Greyson Christoforo, M.; Cui, Y.; McGehee, M. D.; Brongersma, M. L. Self-Limited Plasmonic Welding of Silver Nanowire Junctions. *Nat. Mater.* **2012**, *11* (3), 241−249.
(48) Afshinmanesh, F.; Curto, A. G.; Milaninia, K. M.; Van Hulst, N. F.; Brongersma, M. L. Transparent Metallic Fractal Electrodes for Semiconductor Devices. *Nano Lett.* **2014**, *14* (9), 5068−5074.
(49) Roh, H. S.; Cho, S. H.; Lee, W. J. Study on the Durability against Heat in ITO/Ag-Alloy/ITO Transparent Conductive Multilayer System. *Phys. Status Solidi Appl. Mater. Sci.* **2010**, *207* (7), 1558−1562.
(50) Shen, J. T.; Catrysse, P. B.; Fan, S. Mechanism for Designing Metallic Metamaterials with a High Index of Refraction. *Phys. Rev. Lett.* **2005**, *94* (19), No. 197401.
(51) Verslegers, L.; Catrysse, P. B.; Yu, Z.; White, J. S.; Barnard, E. S.; Brongersma, M. L.; Fan, S. Planar Lenses Based on Nanoscale Slit Arrays in a Metallic Film. *Nano Lett.* **2009**, *9* (1), 235−238.

https://doi.org/10.1021/acsphotonics.3c00693
ACS Photonics XXXX, XXX, XXX−XXX